Received: 24 January 2023 | Revised: 17 May 2023 | Accepted: 29 June 2023

DOI: 10.1002/bit.28492

ARTICLE

BIOTECHNOLOGY AND BIOENGINEERING WILEY

Dynamic metagenome-scale metabolic modeling of a yogurt bacterial community

Sizhe Qiu[1,2] | Hong Zeng[1] | Zhijie Yang[1] | Wei-Lian Hung[3] | Bei Wang[1] | Aidong Yang[2]

[1]School of Food and Health, Beijing Technology and Business University, Beijing, China

[2]Department of Engineering Science, University of Oxford, Oxford, UK

[3]National Center of Technology Innovation for Dairy, China

Correspondence

Bei Wang, School of Food and Health, Beijing Technology and Business University, 100048 Beijing, China.
Email: wangbei@th.btbu.edu.cn

Aidong Yang, Department of Engineering Science, University of Oxford, Oxford OX1 3PJ, UK.
Email: aidong.yang@eng.ox.ac.uk

Funding information

National Center of Technology Innovation for Dairy, Grant/Award Number,
Grant/Award Number: 2021-National Center of Technology Innovation for Dairy-6

Abstract

Genome-scale metabolic models and flux balance analysis (FBA) have been extensively used for modeling and designing bacterial fermentation. However, FBA-based metabolic models that accurately simulate the dynamics of coculture are still rare, especially for lactic acid bacteria used in yogurt fermentation. To investigate metabolic interactions in yogurt starter culture of *Streptococcus thermophilus* and *Lactobacillus delbrueckii* subsp. *bulgaricus*, this study built a dynamic metagenome-scale metabolic model which integrated constrained proteome allocation. The accuracy of the model was evaluated by comparing predicted bacterial growth, consumption of lactose and production of lactic acid with reference experimental data. The model was then used to predict the impact of different initial bacterial inoculation ratios on acidification. The dynamic simulation demonstrated the mutual dependence of *S. thermophilus* and *L. d. bulgaricus* during the yogurt fermentation process. As the first dynamic metabolic model of the yogurt bacterial community, it provided a foundation for the computer-aided process design and control of the production of fermented dairy products.

KEYWORDS

fermentation, genome-scale metabolic model, lactic acid bacteria, metagenomics, proteome allocation

1 | INTRODUCTION

Yogurt is an important fermented dairy product, traditionally made by a starter culture composed of lactic acid bacteria (LAB), such as *Streptococcus thermophilus*, *Lactobacillus delbrueckii* subsp. *bulgaricus*, and *Lactobacillus acidophilus* (Mohammadi et al., 2012). In industrial yogurt production, fermentation process control, in terms of acidification and production of flavor and probiotic compounds, largely depends on the composition of the starter culture. The interactions of LABs affect the fermentation kinetics and thus influence the properties of the yogurt. For example, it was found that the coculture of *S. thermophilus* and *L. delbrueckii* subsp. *bulgaricus* could result in a higher productivity of lactic acid than that of *S. thermophilus* and *L. acidophilus* (Oliveira et al., 2012).

Abbreviations: CDM, chemically defined medium; CFU, colony-forming unit; dFBA, dynamic flux balance analysis; DW, dry weight; FBA, flux balance analysis; GSMM, genome-scale metabolic model; LAB, lactic acid bacteria; LB, *Lactobacillus delbrueckii* subsp. *bulgaricus*; MAG, metagenome-assembled genome; ST, *Streptococcus thermophilus*.

Sizhe Qiu and Hong Zeng contributed equally to this work.

Therefore, designing an optimal yogurt starter culture for desired yogurt properties is one of the primary engineering objectives for yogurt manufacturers.

To investigate and rationally engineer the yogurt starter culture in a more efficient and low-cost manner, a computational model is needed to simulate key variables, such as LAB biomass levels and concentrations of critical compounds, in the fermentation process. There are mainly two types of models for simulating microbial growth and metabolism: differential-equation-based model and flux balance analysis (FBA)-based model. So far, there have been many attempts to use differential-equation-based models to simulate growth, substrate consumption, and lactic acid production of LABs (Bouguettoucha et al., 2011). However, some of these models are too simplistic that only consist of Monod or extended Monod equations that empirically link microbial growth and substrate utilization (Bâati et al., 2004; Vázquez & Murado, 2008; Youssef et al., 2005), leaving the whole metabolic network as a "black box." There also exist differential-equation-based "white box" models that capture the metabolic activity via a series of enzyme kinetic equations (Foster et al., 2021). These models are typically costly to construct due to various enzyme kinetic mechanisms (Ulusu, 2015) and would require a large number of enzyme kinetic parameters that are difficult to obtain (Bar-Even et al., 2011).

Alternatively, FBA-based metabolic models can avoid major shortcomings of differential-equation-based models. First, genome-scale metabolic models (GSMMs) can be easily reconstructed when annotated genomes are available (Mendoza et al., 2019). Second, FBA does not require information on enzyme kinetic mechanisms and kinetic parameters (e.g., k_{cat}) (Orth et al., 2010). Finally, the gene–protein-reaction relations in GSMMs allow the integration of multiomics data, such as quantified proteomics (Bakker et al., 2010). Currently, several GSMMs for dairy-origin LABs have already been reconstructed (Flahaut et al., 2013; Oliveira et al., 2005; Özcan et al., 2019; Pastink et al., 2009), and a dynamic coculture metabolic model for cheese starter culture involving those GSMMs has been built (Özcan et al., 2021). However, there is still a lack of metagenome-scale metabolic models (Branco dos Santos et al., 2013) that can simulate the growth and metabolism of LAB cocultures used in real industrial scenarios (as opposed to assumed ones). Furthermore, existing FBA models of LAB cultures cannot simulate unique interspecies interactions in yogurt fermentation.

With the aim to quantitatively model the fermentation kinetics and metabolic interactions of LABs in yogurt fermentation, this study built the first dynamic metagenome-scale metabolic model of major species identified in the yogurt starter culture, that is, *S. thermophilus* (ST) and *L. delbrueckii* subsp. *bulgaricus* (LB). In addition, constrained proteome allocation, for the first time, was integrated into dynamic community-level FBA. Subsequently, we showed how the model can simulate the growth and metabolism of the ST/LB coculture during yogurt fermentation with good accuracy. Finally, we explored the potential of the developed model in supporting the design and optimization of the yogurt fermentation process via simulating the impact of differential ST/LB inoculation ratio on the overall fermentation behavior.

2 | MATERIALS AND METHODS

2.1 | Sample preparation and fermentation conditions

To conduct the experiment, a commercial yogurt fermentation starter (YoFlex Premium 1.0, CHR Hansen) of pack size 250 U was used. A growth medium was prepared by adding Fonterra whole milk powder to 1 L of water and stirring for 1 h to achieve a 12% (w/w) concentration. The growth medium was then heated to 95°C for 5 min and cooled to 42°C for the inoculation of the fermentation starter. The fermentation process was carried out at a temperature of 43°C for 5 h until the system reached the endpoint at pH = ~ 4.5.

2.2 | Cell counting and pH measurement

To quantify the growth kinetics of bacteria during fermentation, viable cell counting was used. LABs were isolated from samples taken at different time points (0, 30, 60, 90, 105, 120, 150, 180, 240, and 300 min) using the dilution plate method (1:10). The isolated bacteria were then cultured on deMan, Rogosa, and Sharpe agar (AOBOX) and M17 agar (AOBOX) under 37°C anaerobic conditions for 48 h to count the colony-forming units. However, it should be noted that due to the inactivity of bacterial cells under low temperatures in storage, viable cell counting reflected an additive curve of cell activation and cell growth at the lagging and exponential phase, resulting in inaccurate quantification of growth kinetics. Hence, the validation of dynamic simulation in Section 3.3 used reference experimental data from the work of Oliveira et al. (2012) (see Section 3.3 and Supporting Information, Section 2).

The pH change during fermentation was measured using a fermentation monitor (iCinac, AMS) with an Inlab Smart pro-ISM detection electrode (Mettler Toledo). Datapoints were collected at a frequency of three times per minute. Before measurement, the electrode was calibrated with a standard pH calibration solution.

2.3 | Metabolomics quantification

The concentrations of lactic acid and lactose were measured at different time points during fermentation using two different high-performance liquid chromatography (HPLC) systems: HPLC-DAD (Agilent 1260) with a C18 column (250 mm × 4.6 mm, Agilent) and HPLC-RI (Waters 2695-2414) with a Zorbax NH2 column (250 mm × 4.6 mm, Agilent). For lactic acid, samples were centrifuged at 8000*g* for 15 min at 4°C, and the supernatant, after being filtered with 0.22 μm pore size, was measured by HPLC. The injection volume was 10 μL, and the flow rate of the mobile phase (A = 0.1% phosphoric

acid, B = acetonitrile) was 0.5 mL/min. The column temperature was set at 30°C and the detection wavelength was 220 nm. The gradient elution procedure was as follows: 0–4 min, 90%–60% elution A; 4–6 min, 60%–50% elution A; 6–9 min, 50%–80% elution A; 9–15 min, 80%–90% elution A. For lactose, samples were first mixed with 12% TCA and centrifuged at 8000*g* for 15 min in 4°C. The supernatant, after being filtered with 0.22 µm pore size, was measured by HPLC. The injection volume was 10 µL, and the flow rate of the mobile phase was 1 mL/min, with the ratio of acetonitrile to water fixed at 70:30 (v/v). The column and detector temperature were set at 40°C. Lactic acid and lactose concentrations measured in this study were not used to validate the dynamic simulation, as explained in Section 2.2. They were only used to validate predicted lactic acid yield ratios from lactose consumed (Section 3.2), and measured lactic acid concentrations were used to fit a linear function for milk pH (Section 2.4.3).

The concentrations of free amino acids in 12% (w/w) reconstituted milk were measured using ultraperformance liquid chromatography (UPLC) (I-Class, Waters) equipped with a triple quadrupole mass spectrometer (Xevo TQ-S micro, Waters). To prepare the samples, 50% ethanol was added to the milk and then shaken. Next, 10 µL of the shaken samples was mixed with 10 µL of deionized water, 5 µL of D-norleucine (internal standard), and 40 µL of 0.1% formic acid in isopropanol. The samples were centrifuged for 10 min at 10,000*g* in 4°C. The resulting supernatant was then added to boric acid buffer and AccQ Tag solution (Kairos) for derivatization, and filtered using a 0.22-µm pore size filter. The column was UPLC HSS T3 (1.7 µm, 2.1 mm × 150 mm, Waters). The injection volume was 5 µL, and the flow rate of the mobile phase (A = 0.1% formic acid, B = acetonitrile) was 0.5 mL/min. The column temperature was set at 50°C. The mass spectrometer was operated in electrospray ionization mode with an ionization energy of 1.5 kV. The cone voltage was set to 20 V, the desolvation temperature was maintained at 600°C, the desolvation gas flow rate was set to 1000 L/h, and the cone gas flow rate was set to 10 L/h. The gradient elution procedure was as follows: 0–2.5 min, 96%–90% elution A; 2.5–5 min, 90%–72% elution A; 5–6 min, 72%–5% elution A; 6–7 min, 5%–5% elution A; 7–9 min, 5%–96% elution A.

2.4 | Dynamic metabolic model from the metagenome of the yogurt starter culture

Building the dynamic metagenome-scale metabolic model of the yogurt starter culture comprised two steps: (1) from metagenome to annotated protein-coding genes of major species and (2) from coding genes to GSMMs (Figure 1). With the resulting GSMMs, dynamic flux balance analysis (dFBA) was implemented to simulate bacterial growth and metabolism, and predict the change in fermentation behavior by perturbation to initial coculture composition.

2.4.1 | Metagenome assembly, binning, and annotation

DNA extraction of the yogurt starter culture followed the procedure in the metagenomic study of cereal vinegar microbiota by Wu et al. (2017). Three parallel DNA samples were sequenced by Illumina PE150 platform, and the raw data were filtered for high-quality reads by removing adapter overlaps, reads with a quality value lower than 38 and length lower than 350 bp. After the quality control step, the cleaned data were assembled by MEGAHIT (Li et al., 2016) with default parameters.

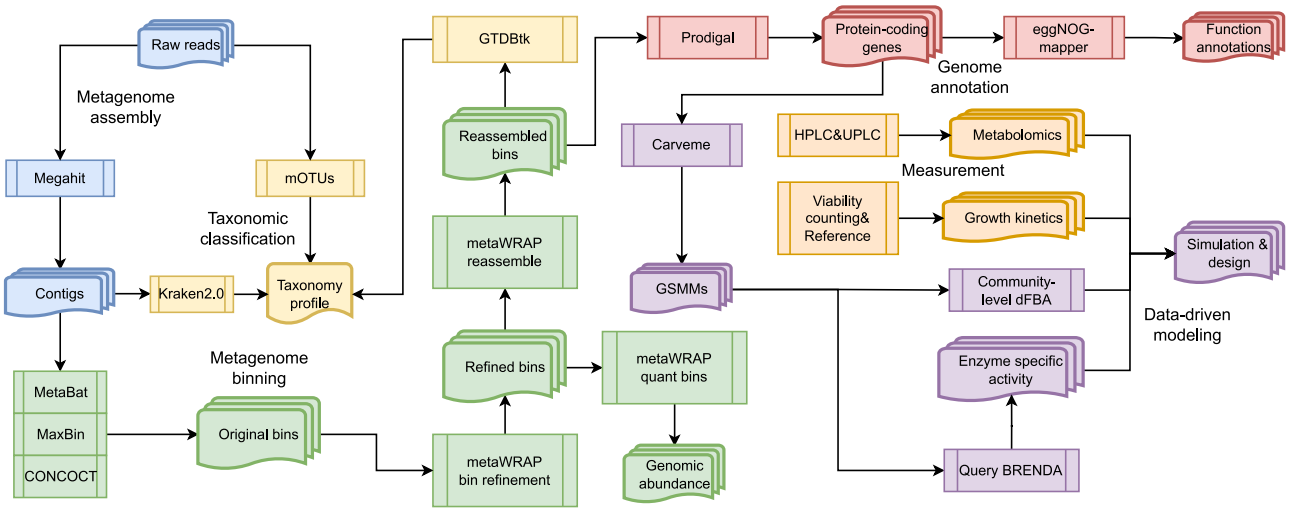

FIGURE 1 Workflow diagram of constructing a dynamic metabolic model for the yogurt starter culture based on metagenomic analysis. CONCOCT, Clustering cONtigs on COverage and ComposiTion; dFBA, dynamic flux balance analysis; GSMM, genome-scale metabolic model; GTDBtk, genome taxonomy database toolkit; HPLC, high-performance liquid chromatography; mOTUs, operational taxonomic units; UPLC, ultraperformance liquid chromatography.

MetaBAT2 (Kang et al., 2019), MaxBin2 (Wu et al., 2016), and CONCOCT (Alneberg et al., 2013) were used for species-level metagenome binning. Then, bins were refined and reassembled using refinement and reassembly modules in metaWRAP (Uritskiy et al., 2018). The final outputs are metagenome-assembled genomes (MAGs) of high quality, assessed by CheckM (Parks et al., 2015). Those bins' genomic abundances in each sample were then computed by the Quant_bin module in metaWRAP.

The taxonomy profile was computed with three different tools. Using reference genomes, operational taxonomic units (mOTUs) identified species and computed relative abundances with unassembled DNA reads (Ruscheweyh et al., 2021). When the metagenome was assembled, KRAKEN-2.0 (Wood et al., 2019) assigned taxonomic labels to DNA reads and generated taxonomic profiles for all samples. Once high-quality bins were generated, genome taxonomy database toolkit (Chaumeil et al., 2019) classified the taxonomy of each bin. Species identified consistently by all taxonomic classification tools were taken as dominant species in the yogurt starter culture.

Protein-coding genes were predicted for each MAG by Prodigal (Hyatt et al., 2010). The functional annotation of protein-coding genes using eggNOG-mapper (Cantalapiedra et al., 2021) was carried out with Kyoto Encyclopedia of Genes and Genomes (KEGG) (Kanehisa et al., 2016) and Carbohydrate-Active enZymes (CAZy) databases (Cantarel et al., 2009), providing information on cellular pathways and CAZy.

2.4.2 | Reconstruction of GSMMs

Nonredundant protein sequences were filtered from concatenated protein sequences of three parallel samples, and used as the input for automatic GSMM reconstruction by CarveMe (Machado et al., 2018). In addition to protein sequences, other inputs were chemically defined media (CDM) for gap filling and the universal bacterial template. The CDM was adopted from the coculture metabolic model of cheese starter in Özcan et al. (2021). The universal bacterial template used for reconstruction was specialized for Gram-positive bacteria.

For refinement of GSMMs, the growth function (biomass synthesis, v_{Growth}) should be set as species-specific (see Supporting Information, Section 1). The stoichiometric coefficients in ST's growth function were adjusted based on measured biomass composition (Pastink et al., 2009), and the growth-associated adenosine triphosphate (ATP) requirement was adopted from the GSMM of *S. thermophilus* CH8 (Rau et al., 2022). Due to data limitation, the biomass composition in LB's growth function was set according to the default of Gram-positive bacteria (Magnúsdóttir et al., 2017), and the growth-associated ATP requirement was adopted from the GSMM of *Lactobacillus plantarum* (Teusink et al., 2006). On the basis of functional annotation of protein-coding genes (Section 2.4.1), reactions included erroneously were removed and missing reactions were added (see Supporting Information, Section 1). In addition, to characterize the proteolysis activity in the coculture system, a self-defined reaction named "*PROLYSIS*" that utilizes the casein peptide was added to the GSMM:

$$\textit{PROLYSIS: Casein peptide}\,(C141H270N35O73S1) \rightarrow \alpha\,\textit{alanine} + \beta\,\textit{arginine} + \cdots + \varepsilon\,\textit{valine}.$$

Stoichiometric coefficients (α, β, ...) in the reaction were approximated from fractions of amino acid in the casein protein of cow milk (Landi et al., 2021) (see Supporting Information, Section 1). The boundary of the flux through casein peptide utilization in each GSMM was set based on the proteolytic activity of each species (see Supporting Information, Section 3 and Figure S3B).

2.4.3 | dFBA and proteome allocation constraint

To simulate the growth of bacteria and the production of target metabolites in time, dFBA was adopted, as a combination of FBA and differential-equation-based dynamic system modeling (Henson & Hanly, 2014). The code of model implementation can be found at https://github.com/SizheQiu/MetaStLbCom. The intracellular metabolic fluxes of a species j were computed by parsimonious FBA, maximizing the growth rate $v_{j,Growth}$ while minimizing the total sum of individual fluxes ($v_{j,i}$ for reaction i in species j), based on the assumption that the cell minimizes the use of enzyme-catalyzed reactions due to the limited cellular recourse (Equations 1 and 2), subject to mass conservation (Equation 3), in which S_j represented the stoichiometric matrix. The concentration change of metabolites and biomass in the extracellular space was modeled by differential equations to account for biomass accumulation (Equation 4) and exchange fluxes of the metabolite e from major species (Equation 5).

$$\textit{Maximize}\ \ v_{j,Growth} \quad \forall\, j \in \textit{major species}, \tag{1}$$

$$\textit{Minimize} \sum_i v_{j,i}, \tag{2}$$

$$S_j v_j = 0, \tag{3}$$

$$\frac{d\,[Biomass_j]}{dt} = v_{j,Growth}\,[Biomass_j], \tag{4}$$

$$\frac{d\,[M\_e]}{dt} = \sum_j v_{j,EX\_M\_e}\,[Biomass_j]. \tag{5}$$

Furthermore, proteome allocation was implemented to constrain reaction fluxes of the central carbon metabolism (Regueira et al., 2021; Zeng & Yang, 2020). Proteome was divided into sectors of inflexible housekeeping (Q), anabolism (A), transportation (T), catabolism (C), and the free sector. The upper bound of all flexible sectors combined was assumed to be 50% of the total proteome (Equations 6 and 7).

The proteome cost on each reaction was computed as the ratio of the flux to the multiplicative product of enzyme activity, a_i, and saturation degree, σ_i (Equation 8). The enzyme saturation degrees (σ_i), except for that of the lactose transporter, are unknown and were set to 0.5, assuming they are similar to glycolytic enzymes in *Escherichia coli* which were reported to be mostly half-saturated (Bennett et al., 2009). For the milk environment, the saturation degree of the lactose transporter (σ_{LT}) was assumed to be 1 as it was considered to be fully saturated by abundant lactose; when the concentration of lactose was low, σ_{LT} was assumed to follow Michaelis–Menten kinetics, $\sigma_{LT} = \frac{[Lactose]}{[Lactose] + K_m}$. The activities of the ribosome for the anabolism sector ($a_{ribosome}$) and acid exportation for lactic and acetic acids (a_{acid_T}) were collected from the literature (Regueira et al., 2021; Schumacher, 2018). Other enzyme activity values were obtained from BRENDA Enzyme Database (Chang et al., 2021) (Table S5). For the uptake of amino acids, the flux was constrained by Michaelis–Menten equation ($\frac{v_{max}[S]}{[S] + K_m}$). The v_{max} of amino acid uptake in ST was obtained from average amino acid uptake upper bounds in Özcan et al. (2021), but for LB, the v_{max} was estimated based on a reported growth rate value on a defined medium (for more details see Supporting Information, Section 3 and Figure S3A). The Michaelis–Menten constant K_m was set based on average parameter values obtained from BRENDA and SABIO-RK (Wittig et al., 2018) (Table S5).

$$\frac{P_{total}}{1\,g\ DW} = p_Q\left(50\%\frac{P_{total}}{1\,g\ DW}\right) + p_C + p_A + p_T + p_{Free}, \tag{6}$$

$$0 < p_C + p_A + p_T \le 50\%\frac{P_{total}}{1\,g\ DW}, \tag{7}$$

$$p_C = \sum\frac{v_i}{\sigma_i a_i}, \quad p_A = \frac{v_{Growth}}{a_{ribosome}}, \quad p_T = \frac{v_{LT}}{\sigma_{LT} a_{LT}} + \frac{v_{acid\_T}}{\sigma_{acid\_T} a_{acid\_T}}. \tag{8}$$

The activity of lactose uptake incorporated inhibition by undissociated lactate (LacH), the product of glycolysis under anaerobic conditions. The exponential decay equation (9) to model the inhibition of lactose transporter activity was adopted from Vereecken and Van Impe (2002) and Aghababaie et al. (2015). The minimal activity of lactose transport a_{LT}^{min} was set to maintain the growth rate at the stationary phase when pH is around 4.5 (see Supporting Information, Section 3 and Figure S3C). The concentration of undissociated lactate was computed using Henderson–Hasselbalch equation (10), $pK_a = 3.86$, and pH was approximated as a linear function of lactic acid concentration, $pH = C_1[Lac] + C_2$ (Figure S1), with measured lactic acid concentrations and pH (Sections 2.2 and 2.3). Such inhibition coefficient, $e^{(-k_{LacH}[LacH])}$, was also applied to amino acid uptake rate and casein peptide utilization rate, and similar to a_{LT}^{min}, the minimal rate, v_{min}, was set (see Supporting Information, Section 3).

$$a_{LT} = \max(a_{LT}^0 e^{(-k_{LacH}[LacH])}, a_{LT}^{min}), \tag{9}$$

$$[LacH] = \frac{[Lac]}{10^{-pK_a}}. \tag{10}$$

3 | RESULTS

3.1 | Metagenomic analysis of the yogurt starter culture

Taxonomic classification by different tools on assembled metagenomes of three samples of the yogurt starter showed that *S. thermophilus* (ST) and *L. delbrueckii* subsp. *bulgaricus* (LB) were two major species that contributed to more than 95% of the overall taxonomy abundance. The genomic abundance ratio of ST and LB in the microbial community was approximately 100:1 (Figure 2a). Detailed taxonomic profiles computed by mOTUs and KRAKEN-2.0 can be found in Table S3. The finalized MAGs, obtained through binning, bin refinement and reassembly, showed high completeness, low contamination, and good continuity (Figure S2). In MAGs of ST and LB from three parallel samples, 2499 and 1801 nonredundant protein-coding genes were identified (Figure 2b), and functionally annotated. KEGG pathway annotation indicated that ST contained a higher amount of genes for amino acid metabolism compared to LB (Figure 2c). In the CAZy annotation, more CAZy were identified in ST's genome, and a significant enrichment of Carbohydrate-Binding Module Family 41 was observed (Figure 2d), which was a module of approximately 100 residues found primarily in bacterial pullulanases (Lammerts van Bueren et al., 2004).

3.2 | Reconstruction of GSMMs with proteome allocation constraints for the yogurt starter culture

Two individual GSMMs for the dominant species in the yogurt starter culture, that is, ST and LB, were reconstructed (see Section 2.4.2). In reconstructed GSMMs, reactions assigned with gene–protein-reaction relations were around 60% in both models. About 25% gap-filled reactions, without genomic basis, were added into the model for a complete metabolic network and the rest were boundary reactions for metabolite exchange (Figure 3a). Classical FBA without additional constraints can only predict an untightened solution space of metabolic fluxes, but fails to account for metabolic capacities of enzymes (Sánchez et al., 2017) and global regulation of proteome sectors (Zeng & Yang, 2020) as described in Section 2.4.3. Therefore, in this study, proteome allocation constraints were integrated into classical FBA to explain the preference for lactic acid production by LABs that is energetically less favorable than acetic acid production. To implement proteome allocation constraints, enzyme activities of reactions in central carbon metabolism were mapped to the reconstructed metabolic network (full names of reactions can be found in Table S4), and proteome costs for producing 1 unit of the flux of lactic acid and acetic acid from pyruvate could be computed (Table S6). The proteome cost of lactic acid production per unit flux is 0.0071 mg E/g DW, the same for ST and LB. For acetic acid, the proteome cost is 0.1218 mg E/g DW in ST, but gets much larger in LB due to the lack of pyruvate formate lyase (PFL), 0.6843 mg E/g DW. In short, the proteome cost of lactic acid

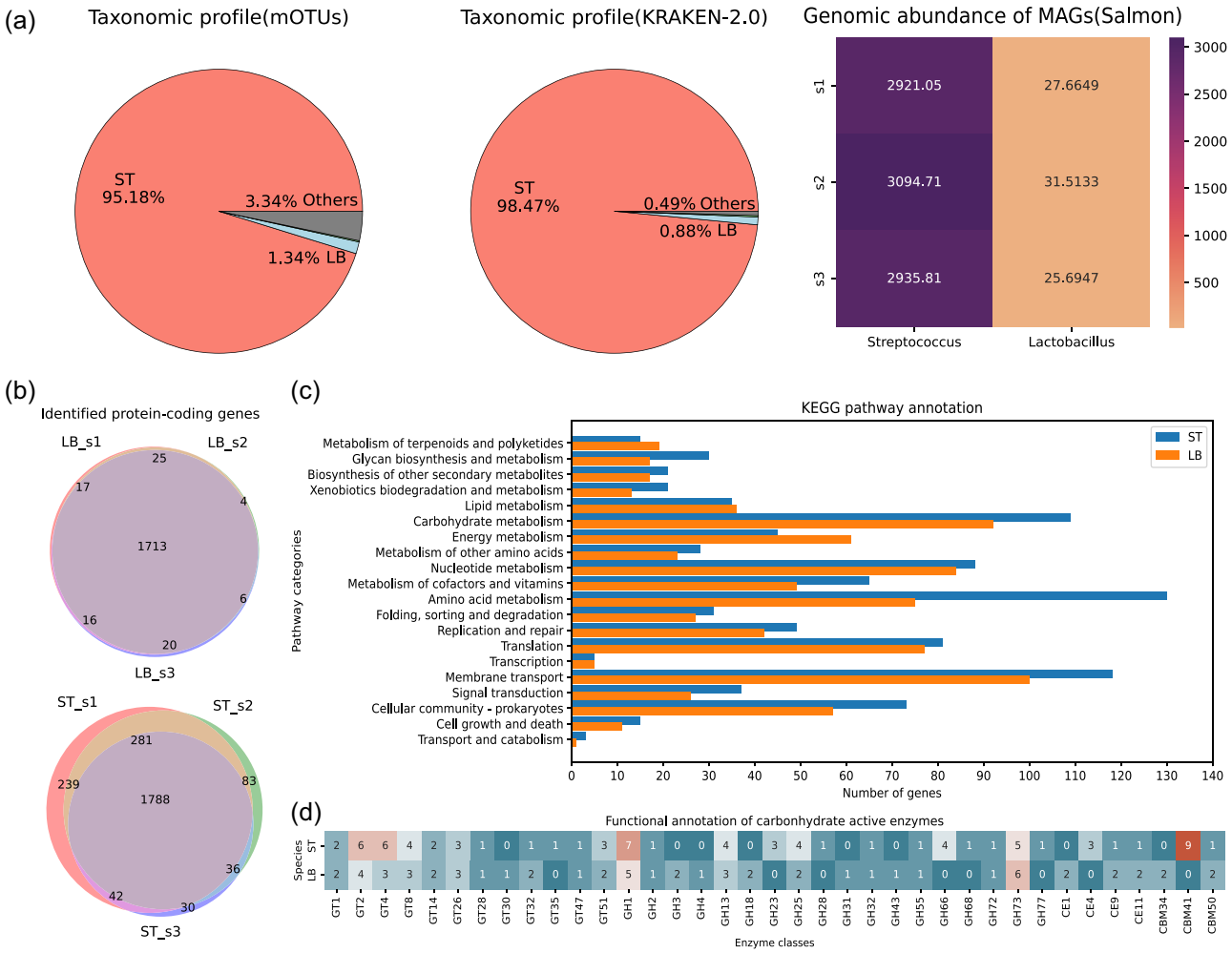

FIGURE 2 Results of metagenomic analysis. (a) Taxonomic classification and genomic abundance, s1–s3: yogurt starter samples 1–3. (b) Pan-genome of identified protein-coding genes from three parallel samples. (c) KEGG pathway and (d) carbohydrate active enzyme annotations for both species. CAZy, Carbohydrate-Active enZymes; KEGG, Kyoto Encyclopedia of Genes and Genomes; LB, *Lactobacillus delbrueckii* subsp. *bulgaricus*; MAG, metagenome-assembled genome; mOTUs, operational taxonomic units; ST, *Streptococcus thermophilus*.

production in LABs is much smaller than that of acetic acid production, though the latter pathway has a higher energy (ATP) yield.

To check the validity of reconstructed GSMMs, FBA with proteome allocation constraints was performed for ST and LB on complete CDM (Rau et al., 2022) and milieu proche du lait (MPL) medium (Chervaux et al., 2000) (Figure 4a,b). For ST, the growth rate reported by Rau et al. (2022) on complete CDM was 0.98 h^{-1} (Rau et al., 2022), and proteome-constrained FBA, with a fixed upper bound of amino acid uptake rate from Özcan et al. (2021), predicted a close value, 1.2 h^{-1}. Due to lack of similar amino acid uptake rate data measured or estimated for LB, the upper bound was estimated in this work by fixing LB's growth rate on MPL medium, reported to be 0.7 h^{-1} (Chervaux et al., 2000) (see Supporting Information, Section 3 and Figure S3A). The predicted lactic acid yield ratio from lactose consumed (mol lactate/mol lactose) was 1.6919 for ST and 1.9305 for LB, which was consistent with the experimental measurement (Table S1) as well as with previous studies (Ghasemi et al., 2009; Özcan et al., 2021; Rau et al., 2022). Due to the lack of PFL (Figure 3b), lb was predicted to have no ability to produce formic acid as well as a much smaller yield of acetic acid compared with ST. Apart from predicting the formation of lactic, acetic, and formic acids, proteome-constrained FBA also predicted the secretion fluxes for various flavor compounds, including 4-hydroxy-benzyl alcohol and succinic acid for ST, and 2-methylbutanoic acid, 2-methylpropanoic acid, 3-methylbutanoic acid, and 2-oxobutanoate for LB (Figure 4a,b).

The predicted responses to the change in the presence of methionine and formic acid by ST and LB show their essential nutrient requirements for cellular growth and potential metabolic interactions (Figure 4c,d). The growth rate of ST increases with the increasing concentrations of methionine (Figure 4c), whereas other amino acids have little impact (Figure S4), suggesting that the GSMM of ST predicts that ST in the starter culture is auxotrophic for methionine and prototrophic for all other 19 essential amino acids. On the other hand, the GSMM of LB reveals its auxotrophy for numerous amino acids (Figure S5), which is consistent with the

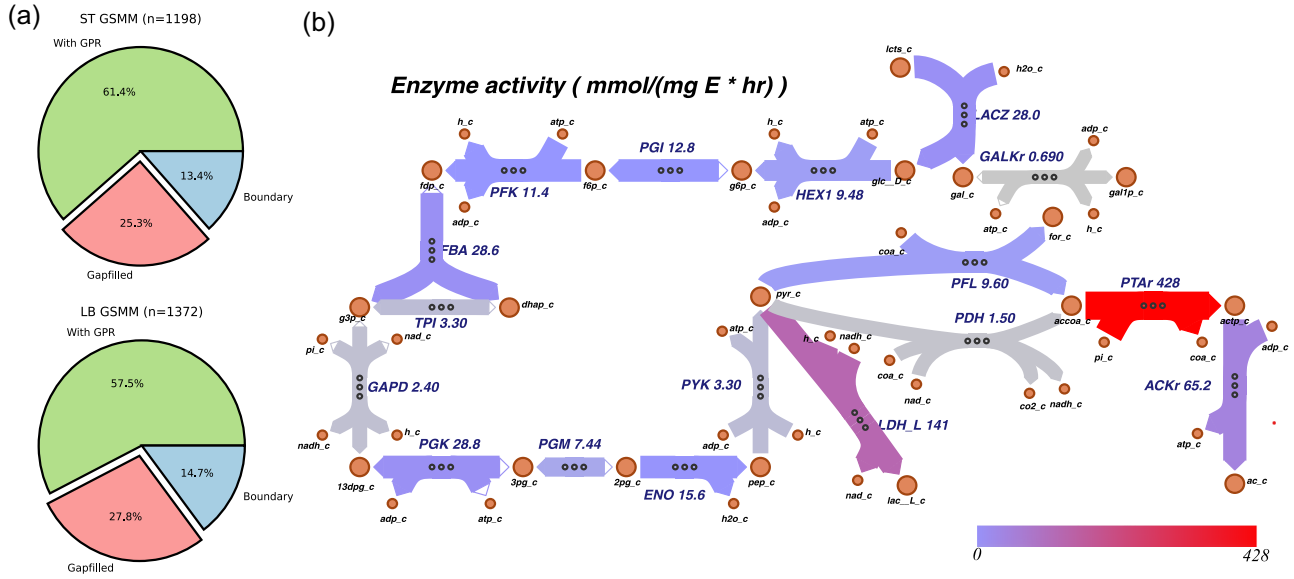

FIGURE 3 Properties of reconstructed GSMMs of the yogurt starter culture. (a) Status of metabolic reaction curation: Green, reactions with gene–protein-reaction rules; Red, reactions that were gap-filled; Blue, exchange reactions at boundary. (b) Enzyme activities mapped to the central carbon metabolic network (full names of reactions can be found in SI, Table S4), only ST has pyruvate formate lyase (PFL) reaction. Big nodes, primary metabolites; small nodes, cofactors. ACKr, acetate kinase; FBA, flux balance analysis; GSMM, genome-scale metabolic model; LB, *Lactobacillus delbrueckii* subsp. *bulgaricus*; LDH, lactate dehydrogenase; PDH, pyruvate dehydrogenase; PTAr, phosphotransacetylase; ST, *Streptococcus thermophilus*.

finding in previous studies that *Lactobacillus* species developed proteolytic ability to compensate for their amino acid auxotrophy (Raveschot et al., 2018). The estimated amino acid auxotrophy in ST and LB by varying amino acid supply is consistent with the auxotrophy calculated by ReFramed (https://github.com/cdanielmachado/reframed) (Machado, 2023). In the in silico milk environment that has no purine (adenine, guanine, and xanthine) to mimic the nutrient composition of actual reconstituted milk used for yogurt fermentation, LB's growth is promoted by the increase of the concentration of formic acid (Figure 4d). In contrast, when purines are supplied, formic acid has little influence on LB's growth rate, which validates the previous finding that LB requires formic acid to synthesize DNA/RNA materials in environments with low levels of purines (Suzuki et al., 1986). Succinctly, the potential metabolic interactions of ST/LB community in the yogurt starter culture inferred by the GSMMs reconstructed in this study can be summarized as the following: ST provides formic acid for LB to synthesize DNA/RNA materials, and LB utilizes casein proteins to supply methionine to ST; they both consume lactose and produce lactic acid, which in turn inhibits their growth (Vereecken & Van Impe, 2002) (Figure 4e).

The addition of proteome constraints allows the model to account for the metabolic switch from acetic acid production to lactic acid production in ST when its growth rate increases with the increase of carbon source concentration, which has been demonstrated in Regueira et al. (2021) with a generic LAB-GSMM that can respond to the change of glucose concentration (Regueira et al., 2021) (Figure 4f,g). The proteome costs allocated to acetate and lactate productions are computed as the proteome cost of PFL, pyruvate dehydrogenase (PDH), phosphotransacetylase, and acetate kinase, and that of lactate dehydrogenase (Figure 4h). In general, only two moles of lactic acid can be produced from the fermentation of one mole of lactose. The predicted ratio of acetic acid produced to lactose consumed sometimes exceeds 2, which results from the metabolism of other nutrients in the in silico culture medium (Figure S6). With LB's GSMM, proteome-constrained FBA could not demonstrate a growth rate triggered a metabolic switch from acetic acid production to lactic acid production due to the much larger protein requirement of converting pyruvate to acetyl-CoA by solely PDH in LB (Figure 3b) and the biosynthetic requirement of fatty acids (Figure S7). When the uptake of lactose provides enough carbon flux that exceeds the biosynthetic requirement of fatty acid, a surplus flux will be predicted to go through acetic acid production (Figure S7).

3.3 | Dynamic simulation of growth kinetics and metabolism of ST/LB coculture

The dynamic simulation of yogurt fermentation was performed using the initial conditions of the coculture experiment in Oliveira et al. (2012). The simulation was validated by comparison with reference experimental data of bacterial biomass, lactose, and lactic acid concentrations, also from Oliveira et al. (2012) (for more details see Supporting Information, Section 2). The accuracy of the simulation was assessed and demonstrated by R^2 values, which were all around 0.8 (Figure 5a–d).

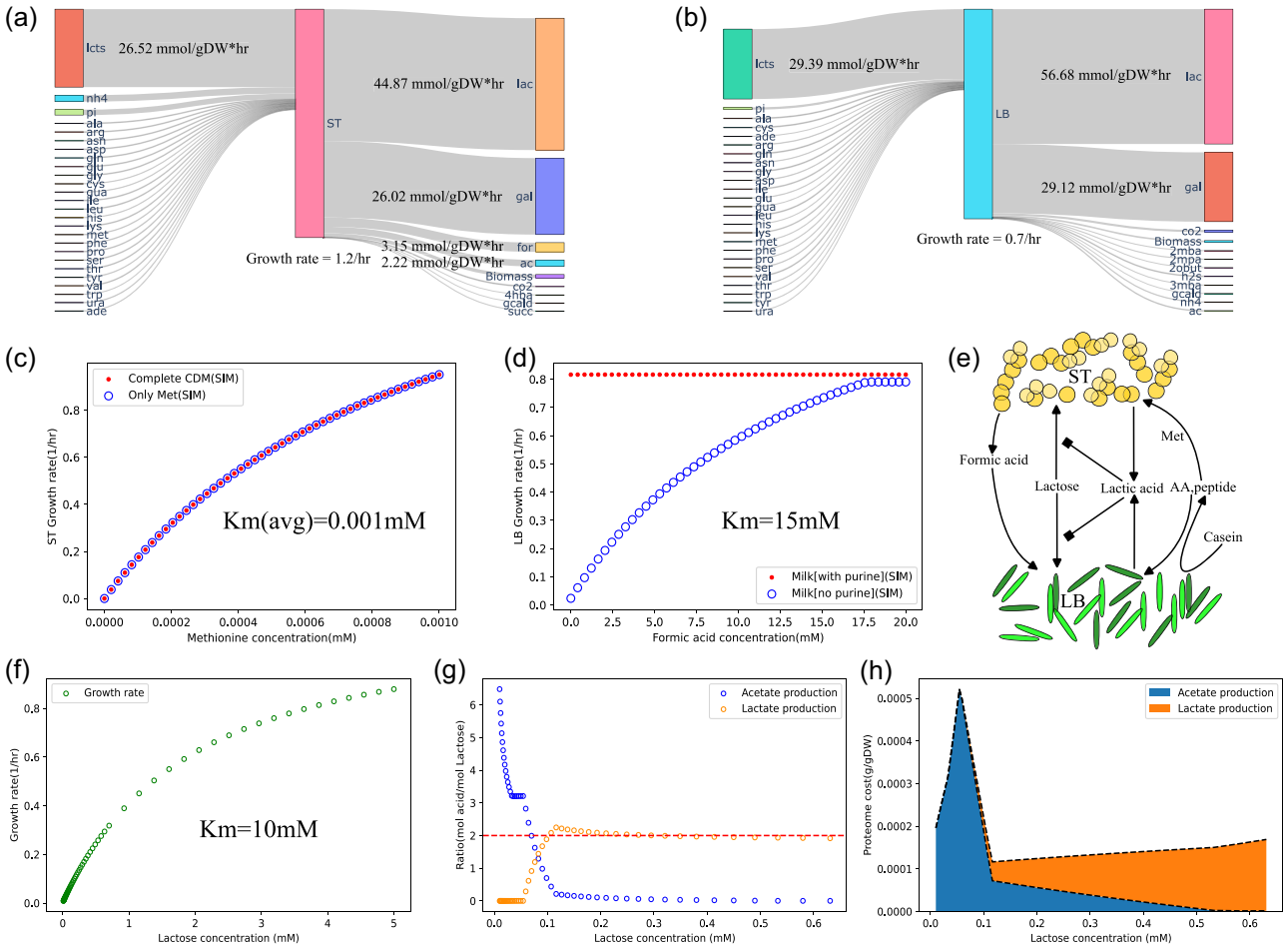

FIGURE 4 Model predictions of the metabolic fluxes on the chemically defined medium. (a, b) Predicted uptake and secretion fluxes of (a) ST on complete CDM and (b) LB on MPL medium. (c, d) Assessment of (c) the requirement of methionine by ST (v_{max} (*average*) = 0.2 mmol/g DW h, Kaiser et al., 2015; K_m (*average*) = 0.001 mM, Özcan et al., 2021) and (d) the requirement of formic acid by LB (v_{max} = 0.3 mmol/g DW h, K_m = 15 mM; Schmidt & Beitz, 2022). SIM, simulation is shown in dotted lines. (e) Potential metabolic interactions of ST/LB coculture. (f–h) The response of ST to the increase of lactose concentration (K_m = 10 mM; Poolman et al., 1995): (e) predicted growth rates, (g) fluxes through acetic/lactic acid productions, and (h) proteome costs allocated to biosynthetic pathways of acetic and lactic acids. 2mba, 2-methylbutanoic acid; 2mpa, 2-methylpropanoic acid; 2obut, 2-oxobutanoate; 3mba, 3-methylbutanoic acid; 4hba, 4-hydroxy-benzyl alcohol; CDM, chemically defined medium; LB, *Lactobacillus delbrueckii* subsp. *bulgaricus*; MPL, milieu proche du lait; MPL, milieu proche du lait; ST, *Streptococcus thermophilus*; succ, succinic acid.

Overall, the model, without parameter recalibration using the reference experimental data, adequately captured the initiation of the exponential growth phase and the transition to the stationary phase for both ST and LB, as well as the protocooperation between the two species (Figure 5a,b). The accumulation of formic acid (produced by ST) initiates the exponential growth of LB by activating its synthesis of purines, whose natural concentration is too low to support the growth of LB in the milk environment. In return, the activation of growth and metabolism of LB with strong proteolytic activity enhances the growth rate of ST by supplementing methionine, which is also limited in the milk environment (Figure 5e,f). With the accumulation of lactic acid, the growth rates of ST and LB are both progressively inhibited. Finally, their growths are halted, as shown by the stationary phase (Figure 5a–c).

3.4 | Prediction of the impact of different initial ST/LB inoculation ratios on the fermentation behavior

Perturbations on the initial inoculation ratio of ST and LB of the yogurt starter culture were conducted to investigate its impact on the fermentation behavior. The total initial biomass concentration of the coculture was fixed at 0.18 g dry weight (DW)/L, the same as the initial condition setting in Section 3.3. The simulated growth curves of ST and LB from different initial ST/LB inoculation ratios demonstrate the mutual dependence of ST and LB in the coculture (Figure 6a). When the initial ST:LB inoculation ratio is modulated to increase from 1 to 10, the proteolytic activity of the microbial community becomes weaker due to the decrease of the initial biomass concentration of LB, and correspondingly, the growth of ST is also reduced due to lowered supply of methionine; When the initial

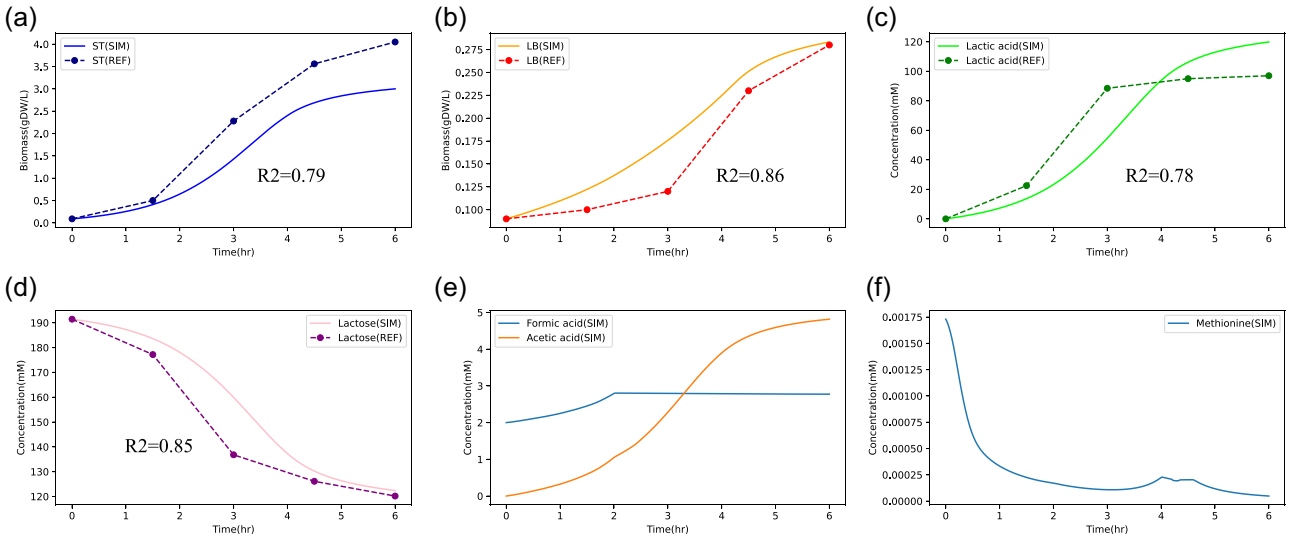

FIGURE 5 Dynamic simulation results of ST/LB coculture (*I. C.* $[Biomass_{ST}] = [Biomass_{LB}] = 0.09$ g DW/L). Comparison between simulated and experimental growth kinetics of ST, $R^2 = 0.79$ (a), and LB, $R^2 = 0.86$ (b). Comparison between simulated and experimental concentration profiles of lactic acid, $R^2 = 0.78$ (c), and lactose, $R^2 = 0.85$ (d). Simulated concentration profiles of formic acid, acetic acid (e), and methionine (f). I.C., initial condition; LB, *Lactobacillus delbrueckii* subsp. *bulgaricus*; REF, reference data shown in dotted lines; SIM, simulation shown in solid lines; ST, *Streptococcus thermophilus*.

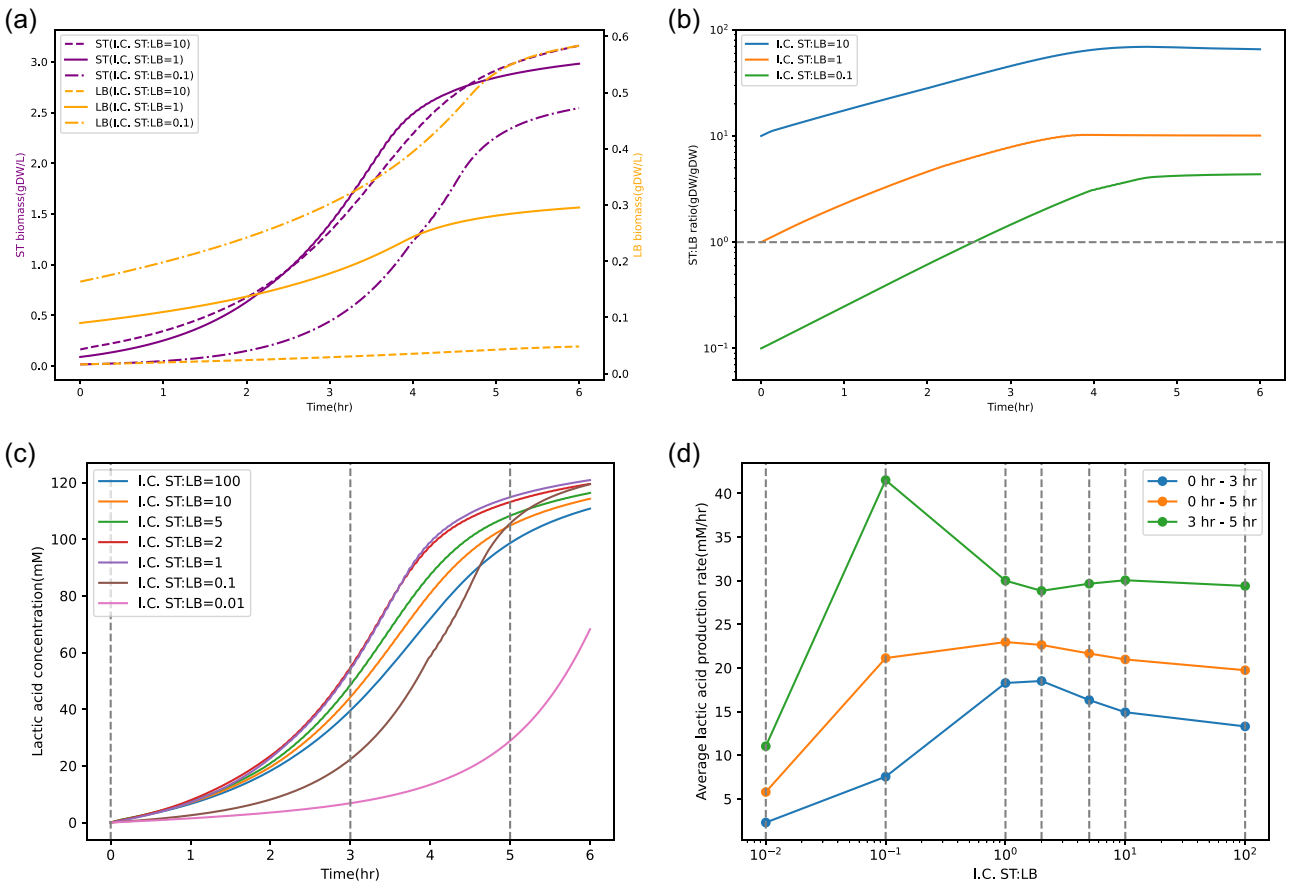

FIGURE 6 Predicted growth kinetics of ST/LB coculture and lactic acid production with different initial ST:LB inoculation ratios. (a) Biomass concentration profiles of ST and LB. (b) Bacterial community composition dynamics: the change of ST/LB ratio in time. Purple, ST; orange, LB; dashed line, I.C. ST:LB = 10; solid line, I.C. ST:LB = 1; dot dash line, I.C. ST:LB = 0.1. (c) Lactic acid concentration profiles for different initial ST/LB inoculation ratios. (d) The assessment of acidification rate for different initial ST/LB inoculation ratios with lactic acid levels at early stage ($T = 3$ h), and later stage ($T = 5$ h). I.C., initial condition; LB, *Lactobacillus delbrueckii* subsp. *bulgaricus*; ST, *Streptococcus thermophilus*.

ST:LB inoculation ratio is set to decrease from 1 to 0.1, the lowered productivity of formic acid from ST makes LB enter the exponential phase slower than that of the case with initial ST:LB = 1 (Figure 6a). In addition, the simulation shows that, given a certain range of initial ST:LB ratios (in this case, 0.1–10), ST will eventually become the dominant species (Figure 6b), which agrees with the previous study on the rods (LB) to cocci (ST) ratio in cheese fermentation (Yun et al., 1995).

The predicted average acidification rates (lactic acid concentration/total fermentation time) in 5 h by different starter culture compositions rank as follows: ST:LB = 1 > ST:LB = 2 > ST:LB = 5 > ST:LB = 10 > ST:LB = 0.1 > ST:LB = 100 > ST:LB = 0.01 (Figure 6c,d). At the early stage of yogurt fermentation (0–3 h), starter cultures with the initial ST:LB ratio larger than 1 have more than twice the lactic acid production rates, in contrast to starter cultures with the initial ST:LB ratio lower than 1; later (3–5 h), the lactic acid production rate of the starter culture with initial ST:LB = 0.1 catches up (Figure 6d). To sum up, initial ST:LB = 1 is predicted to be optimal for lactic acid production in 5 h if the initial total biomass is fixed at 0.18 g DW/L, and the acidification will generally be faster initially when ST is the dominant species in the coculture. On the basis of predicted acidification kinetics, the starter culture composition can be designed for targeted acidification patterns, for example, ST:LB ratio = 0.1 is suitable for slow acidification first but fast acidification later.

4 | DISCUSSION

Overall, this work presented the reconstruction of GSMMs for the yogurt starter culture, that is, the coculture of ST and LB, based on metagenomic analysis and provided a dynamic metagenome-scale metabolic modeling approach for simulating the microbial growth and metabolism during the yogurt fermentation process. Although community-level FBA has already been used in a few scenarios to simulate growth and metabolism (Branco dos Santos et al., 2013; Khandelwal et al., 2013; Sieuwerts, 2009), the model in this study, for the first time, integrated constrained proteome allocation into dynamic community-level FBA. Different from the direct integration of gene expression data into FBA, such as the work of Blasche et al. (2021), the proteome allocation constraint aims to capture the process of redistribution of proteome resources to each cellular pathway at different growth stages; it does not directly incorporate gene expression data into the model but tightens the solution space of fluxes by setting a global constraint on the metabolic capacity. Also, this model introduced feed-back inhibition function on the enzyme activity, previously used in modeling growth kinetics of LABs (Vereecken & Van Impe, 2002), and effectively simulated the product inhibition by undissociated lactic acid on the growth of LABs (Section 3.3). The proposed dynamic model quantitatively demonstrated the metabolic mutual dependence of ST and LB in the milk environment (Oliveira et al., 2012; Sieuwerts, 2009), and provided confirmation of such ecological interaction with data-driven modeling.

Although the model showed good predictive accuracy in bacterial growth and metabolism (Sections 3.2 and 3.3), it had limitations in mainly three aspects: (1) MAG-derived GSMMs of ST and LB lacked accurate strain-specific biomass compositions and growth-associated ATP requirements; (2) the model could not yet predict fluxes through the biosynthesis of important flavor compounds, such as methyl ketones, and the probiotic exopolysaccharides that are often produced in yogurt fermentation; (3) no mechanistic representation of regulatory activities was included in the current model. For instance, acidification by ST was previously found to be stimulated by formic acid, casitone, pyruvic acid, folic acid, and polysorbate 20 (Sieuwerts et al., 2010). Monoculture of dominant ST and LB strains separated from the starter culture will be needed to approximate the growth-associated ATP requirement from the carbon source utilized (Teusink et al., 2006), and gas chromatography/mass spectrometry or HPLC can be used to quantify major components in cellular biomass, that is, protein, DNA, RNA, lipids, and glycogen (Long & Antoniewicz, 2014; Simensen et al., 2022). To resolve the other two limitations, the proposed next step is to further refine the established GSMMs by manually adding the biosynthetic pathways of flavor and probiotic compounds of interests and implement dynamic regulatory FBA (Liu & Bockmayr, 2020) with meta-transcriptome profiling. For the current model, the failure to predict active fluxes towards the formation of diacetyl and acetoin was not caused by the lack of pathway reconstruction, but the lack of a constraint to divert the downstream metabolic flux to those biomass-independent products.

Despite those several limitations remain to be overcome, the genome-scale metabolic reconstructions and the dynamic community-level FBA model for the classical yogurt starter culture of ST and LB presented in this work have been shown to have the potential to offer an efficient tool to guide engineering decisions in fermentation processes, which could be used to address issues such as the optimal initial biomass ratio of ST and LB to maximize the rate of acidification or possibly other process targets (e.g., flavor formation). Furthermore, the two-species model can be expanded by including GSMMs of other probiotic bacteria, for example, bifidobacterium (Lamoureux et al., 2002), to simulate the fermentation dynamics of more complex starter cultures.

AUTHOR CONTRIBUTIONS

Sizhe Qiu and Hong Zeng contributed equally to this work. All authors contributed to the study conception and design. Sizhe Qiu contributed to the metagenomic analysis and model development. Sizhe Qiu and Hong Zeng jointly contributed to the analysis and interpretation of results and manuscript preparation. Zhijie Yang performed the biochemical analysis of the coculture. Wei-Lian Hung, Bei Wang and Aidong Yang critically revised the manuscript. All authors reviewed the results and approved the final version of the manuscript.

ACKNOWLEDGMENTS

The authors would like to acknowledge the financial support provided by the National Center of Technology Innovation for Dairy under Grant No. 2021-National Center of Technology Innovation for Dairy-6. Additionally, the authors would like to express their gratitude to Dr. Baochao Hou for offering expert advice in the analysis of the yogurt starter culture.

CONFLICT OF INTEREST STATEMENT

The authors declare no conflict of interest.

DATA AVAILABILITY STATEMENT

The data that support the findings of this study are openly available in MetaStLbCom at https://github.com/SizheQiu/MetaStLbCom.

ORCID

Sizhe Qiu http://orcid.org/0000-0002-1936-1223

REFERENCES

Aghababaie, M., Khanahmadi, M., & Beheshti, M. (2015). Developing a kinetic model for co-culture of yogurt starter bacteria growth in pH controlled batch fermentation. *Journal of Food Engineering*, *166*, 72–79. https://doi.org/10.1016/j.jfoodeng.2015.05.013

Alneberg, J., Bjarnason, B. S., de Bruijn, I., Schirmer, M., Quick, J., Ijaz, U. Z., Loman, N. J., Andersson, A. F., & Quince, C. (2013). CONCOCT: Clustering cONtigs on COverage and ComposiTion. http://arxiv.org/abs/1312.4038

Bâati, L., Roux, G., Dahhou, B., & Uribelarrea, J.-L. (2004). Unstructured modelling growth of *Lactobacillus acidophilus* as a function of the temperature. *Mathematics and Computers in Simulation*, *65*(1), 137–145. https://doi.org/10.1016/j.matcom.2003.09.013

Bakker, B. M., van Eunen, K., Jeneson, J. A. L., van Riel, N. A. W., Bruggeman, F. J., & Teusink, B. (2010). Systems biology from microorganisms to human metabolic diseases: The role of detailed kinetic models. *Biochemical Society Transactions*, *38*(5), 1294–1301. https://doi.org/10.1042/BST0381294

Bar-Even, A., Noor, E., Savir, Y., Liebermeister, W., Davidi, D., Tawfik, D. S., & Milo, R. (2011). The moderately efficient enzyme: Evolutionary and physicochemical trends shaping enzyme parameters. *Biochemistry*, *50*(21), 4402–4410. https://doi.org/10.1021/bi2002289

Bennett, B. D., Kimball, E. H., Gao, M., Osterhout, R., Van Dien, S. J., & Rabinowitz, J. D. (2009). Absolute metabolite concentrations and implied enzyme active site occupancy in *Escherichia coli*. *Nature Chemical Biology*, *5*(8), 593–599. https://doi.org/10.1038/nchembio.186

Blasche, S., Kim, Y., Mars, R. A. T., Machado, D., Maansson, M., Kafkia, E., Milanese, A., Zeller, G., Teusink, B., Nielsen, J., Benes, V., Neves, R., Sauer, U., & Patil, K. R. (2021). Metabolic cooperation and spatiotemporal niche partitioning in a kefir microbial community. *Nature Microbiology*, *6*(2), 196–208. https://doi.org/10.1038/s41564-020-00816-5

Bouguettoucha, A., Balannec, B., & Amrane, A. (2011). Unstructured models for lactic acid fermentation—A review. *Food Technology and Biotechnology*, *49*(1), 3. https://www.researchgate.net/profile/Abdallah-Bouguettoucha/publication/228355166_Unstructured_Models_for_Lactic_Acid_Fermentation-A_Review/links/02e7e53bedb3eb05fe000000/Unstructured-Models-for-Lactic-Acid-Fermentation-A-Review.pdf

Branco dos Santos, F., de Vos, W. M., & Teusink, B. (2013). Towards metagenome-scale models for industrial applications—The case of lactic acid bacteria. *Current Opinion in Biotechnology*, *24*(2), 200–206. https://doi.org/10.1016/j.copbio.2012.11.003

Cantalapiedra, C. P., Hernández-Plaza, A., Letunic, I., Bork, P., & Huerta-Cepas, J. (2021). eggNOG-mapper v2: Functional annotation, orthology assignments, and domain prediction at the metagenomic scale. *Molecular Biology and Evolution*, *38*(12), 5825–5829. https://doi.org/10.1093/molbev/msab293

Cantarel, B. L., Coutinho, P. M., Rancurel, C., Bernard, T., Lombard, V., & Henrissat, B. (2009). The Carbohydrate-Active enZymes database (CAZy): An expert resource for glycogenomics. *Nucleic Acids Research*, *37*(Database issue), D233–D238. https://doi.org/10.1093/nar/gkn663

Chang, A., Jeske, L., Ulbrich, S., Hofmann, J., Koblitz, J., Schomburg, I., Neumann-Schaal, M., Jahn, D., & Schomburg, D. (2021). BRENDA, the ELIXIR core data resource in 2021: New developments and updates. *Nucleic Acids Research*, *49*(D1), D498–D508. https://doi.org/10.1093/nar/gkaa1025

Chaumeil, P.-A., Mussig, A. J., Hugenholtz, P., & Parks, D. H. (2019). GTDB-Tk: A toolkit to classify genomes with the genome taxonomy database. *Bioinformatics (Oxford, England)*, *36*, 1925–1927. https://doi.org/10.1093/bioinformatics/btz848

Chervaux, C., Ehrlich, S. D., & Maguin, E. (2000). Physiological study of *Lactobacillus delbrueckii* subsp. *bulgaricus* strains in a novel chemically defined medium. *Applied and Environmental Microbiology*, *66*(12), 5306–5311. https://doi.org/10.1128/AEM.66.12.5306-5311.2000

Flahaut, N. A. L., Wiersma, A., van de Bunt, B., Martens, D. E., Schaap, P. J., Sijtsma, L., Dos Santos, V. A. M., & de Vos, W. M. (2013). Genome-scale metabolic model for *Lactococcus lactis* MG1363 and its application to the analysis of flavor formation. *Applied Microbiology and Biotechnology*, *97*(19), 8729–8739. https://doi.org/10.1007/s00253-013-5140-2

Foster, C. J., Wang, L., Dinh, H. V., Suthers, P. F., & Maranas, C. D. (2021). Building kinetic models for metabolic engineering. *Current Opinion in Biotechnology*, *67*, 35–41. https://doi.org/10.1016/j.copbio.2020.11.010

Ghasemi, M., Najafpour, G., Rahimnejad, M., Beigi, P. A., Sedighi, M., & Hashemiyeh, B. (2009). Effect of different media on production of lactic acid from whey by *Lactobacillus bulgaricus*. *African Journal of Biotechnology*, *8*(1), 81–84. https://doi.org/10.4314/ajb.v8i1.59741

Henson, M. A., & Hanly, T. J. (2014). Dynamic flux balance analysis for synthetic microbial communities. *IET Systems Biology*, *8*(5), 214–229. https://doi.org/10.1049/iet-syb.2013.0021

Hyatt, D., Chen, G.-L., Locascio, P. F., Land, M. L., Larimer, F. W., & Hauser, L. J. (2010). Prodigal: Prokaryotic gene recognition and translation initiation site identification. *BMC Bioinformatics*, *11*, 119. https://doi.org/10.1186/1471-2105-11-119

Kaiser, J. C., Omer, S., Sheldon, J. R., Welch, I., & Heinrichs, D. E. (2015). Role of BrnQ1 and BrnQ2 in branched-chain amino acid transport and virulence in *Staphylococcus aureus*. *Infection and Immunity*, *83*(3), 1019–1029. https://doi.org/10.1128/IAI.02542-14

Kanehisa, M., Sato, Y., Kawashima, M., Furumichi, M., & Tanabe, M. (2016). KEGG as a reference resource for gene and protein annotation. *Nucleic Acids Research*, *44*(D1), D457–D462. https://doi.org/10.1093/nar/gkv1070

Kang, D. D., Li, F., Kirton, E., Thomas, A., Egan, R., An, H., & Wang, Z. (2019). MetaBAT 2: An adaptive binning algorithm for robust and efficient genome reconstruction from metagenome assemblies. *PeerJ*, *7*, e7359. https://doi.org/10.7717/peerj.7359

Khandelwal, R. A., Olivier, B. G., Röling, W. F. M., Teusink, B., & Bruggeman, F. J. (2013). Community flux balance analysis for microbial consortia at balanced growth. *PLoS ONE*, *8*(5), e64567. https://doi.org/10.1371/journal.pone.0064567

Lammerts van Bueren, A., Finn, R., Ausió, J., & Boraston, A. B. (2004). α-Glucan recognition by a new family of carbohydrate-binding modules found primarily in bacterial pathogens. *Biochemistry*, *43*(49), 15633–15642. https://doi.org/10.1021/bi048215z

Lamoureux, L., Roy, D., & Gauthier, S. F. (2002). Production of oligosaccharides in yogurt containing bifidobacteria and yogurt cultures. *Journal of Dairy Science*, *85*(5), 1058–1069. https://doi.org/10.3168/jds.S0022-0302(02)74166-0

Landi, N., Ragucci, S., & Di Maro, A. (2021). Amino acid composition of milk from cow, sheep and goat raised in Ailano and Valle Agricola, two localities of "Alto Casertano" (Campania region). *Foods (Basel, Switzerland)*, *10*(10), 2431. https://doi.org/10.3390/foods10102431

Li, D., Luo, R., Liu, C.-M., Leung, C.-M., Ting, H.-F., Sadakane, K., Yamashita, H., & Lam, T.-W. (2016). MEGAHIT v1.0: A fast and scalable metagenome assembler driven by advanced methodologies and community practices. *Methods*, *102*, 3–11. https://doi.org/10.1016/j.ymeth.2016.02.020

Liu, L., & Bockmayr, A. (2020). Regulatory dynamic enzyme-cost flux balance analysis: A unifying framework for constraint-based modeling. *Journal of Theoretical Biology*, *501*, 110317. https://doi.org/10.1016/j.jtbi.2020.110317

Long, C. P., & Antoniewicz, M. R. (2014). Quantifying biomass composition by gas chromatography/mass spectrometry. *Analytical Chemistry*, *86*(19), 9423–9427. https://doi.org/10.1021/ac502734e

Machado, D. (2023). *reframed: ReFramed: Metabolic modeling package*. Github. https://github.com/cdanielmachado/reframed

Machado, D., Andrejev, S., Tramontano, M., & Patil, K. R. (2018). Fast automated reconstruction of genome-scale metabolic models for microbial species and communities. *Nucleic Acids Research*, *46*(15), 7542–7553. https://doi.org/10.1093/nar/gky537

Magnúsdóttir, S., Heinken, A., Kutt, L., Ravcheev, D. A., Bauer, E., Noronha, A., Greenhalgh, K., Jäger, C., Baginska, J., Wilmes, P., Fleming, R. M. T., & Thiele, I. (2017). Generation of genome-scale metabolic reconstructions for 773 members of the human gut microbiota. *Nature Biotechnology*, *35*(1), 81–89. https://doi.org/10.1038/nbt.3703

Mendoza, S. N., Olivier, B. G., Molenaar, D., & Teusink, B. (2019). A systematic assessment of current genome-scale metabolic reconstruction tools. *Genome Biology*, *20*(1), 158. https://doi.org/10.1186/s13059-019-1769-1

Mohammadi, R., Sohrabvandi, S., & Mohammad Mortazavian, A. (2012). The starter culture characteristics of probiotic microorganisms in fermented milks. *Engineering in Life Sciences*, *12*(4), 399–409. https://doi.org/10.1002/elsc.201100125

Oliveira, A. P., Nielsen, J., & Förster, J. (2005). Modeling *Lactococcus lactis* using a genome-scale flux model. *BMC Microbiology*, *5*, 39. https://doi.org/10.1186/1471-2180-5-39

Oliveira, R. P. S., Torres, B. R., Perego, P., Oliveira, M. N., & Converti, A. (2012). Co-metabolic models of *Streptococcus thermophilus* in co-culture with *Lactobacillus bulgaricus* or *Lactobacillus acidophilus*. *Biochemical Engineering Journal*, *62*, 62–69. https://doi.org/10.1016/j.bej.2012.01.004

Orth, J. D., Thiele, I., & Palsson, B. Ø. (2010). What is flux balance analysis? *Nature Biotechnology*, *28*(3), 245–248. https://doi.org/10.1038/nbt.1614

Özcan, E., Selvi, S. S., Nikerel, E., Teusink, B., Toksoy Öner, E., & Çakır, T. (2019). A genome-scale metabolic network of the aroma bacterium *Leuconostoc mesenteroides* subsp. *cremoris*. *Applied Microbiology and Biotechnology*, *103*(7), 3153–3165. https://doi.org/10.1007/s00253-019-09630-4

Özcan, E., Seven, M., Şirin, B., Çakır, T., Nikerel, E., Teusink, B., & Toksoy Öner, E. (2021). Dynamic co-culture metabolic models reveal the fermentation dynamics, metabolic capacities and interplays of cheese starter cultures. *Biotechnology and Bioengineering*, *118*(1), 223–237. https://doi.org/10.1002/bit.27565

Parks, D. H., Imelfort, M., Skennerton, C. T., Hugenholtz, P., & Tyson, G. W. (2015). CheckM: Assessing the quality of microbial genomes recovered from isolates, single cells, and metagenomes. *Genome Research*, *25*(7), 1043–1055. https://doi.org/10.1101/gr.186072.114

Pastink, M. I., Teusink, B., Hols, P., Visser, S., de Vos, W. M., & Hugenholtz, J. (2009). Genome-scale model of *Streptococcus thermophilus* LMG18311 for metabolic comparison of lactic acid bacteria. *Applied and Environmental Microbiology*, *75*(11), 3627–3633. https://doi.org/10.1128/AEM.00138-09

Poolman, B., Knol, J., & Lolkema, J. S. (1995). Kinetic analysis of lactose and proton coupling in Glu379 mutants of the lactose transport protein of *Streptococcus thermophilus*. *Journal of Biological Chemistry*, *270*(22), 12995–13003. https://doi.org/10.1074/jbc.270.22.12995

Rau, M. H., Gaspar, P., Jensen, M. L., Geppel, A., Neves, A. R., & Zeidan, A. A. (2022). Genome-scale metabolic modeling combined with transcriptome profiling provides mechanistic understanding of *Streptococcus thermophilus* CH8 metabolism. *Applied and Environmental Microbiology*, *88*(16), e0078022. https://doi.org/10.1128/aem.00780-22

Raveschot, C., Cudennec, B., Coutte, F., Flahaut, C., Fremont, M., Drider, D., & Dhulster, P. (2018). Production of bioactive peptides by *Lactobacillus* species: From gene to application. *Frontiers in Microbiology*, *9*, 2354. https://doi.org/10.3389/fmicb.2018.02354

Regueira, A., Rombouts, J. L., Wahl, S. A., Mauricio-Iglesias, M., Lema, J. M., & Kleerebezem, R. (2021). Resource allocation explains lactic acid production in mixed-culture anaerobic fermentations. *Biotechnology and Bioengineering*, *118*(2), 745–758. https://doi.org/10.1002/bit.27605

Ruscheweyh, H.-J., Milanese, A., Paoli, L., Sintsova, A., Mende, D. R., Zeller, G., & Sunagawa, S. (2021). mOTUs: Profiling taxonomic composition, transcriptional activity and strain populations of microbial communities. *Current Protocols*, *1*(8), e218. https://doi.org/10.1002/cpz1.218

Sánchez, B. J., Zhang, C., Nilsson, A., Lahtvee, P.-J., Kerkhoven, E. J., & Nielsen, J. (2017). Improving the phenotype predictions of a yeast genome-scale metabolic model by incorporating enzymatic constraints. *Molecular Systems Biology*, *13*(8), 935. https://doi.org/10.15252/msb.20167411

Schmidt, J. D. R., & Beitz, E. (2022). Mutational widening of constrictions in a formate–nitrite/H+ transporter enables aquaporin-like water permeability and proton conductance. *Journal of Biological Chemistry*, *298*(1), 101513. https://doi.org/10.1016/j.jbc.2021.101513

Schumacher, R. (2018). *Metabolic trade-offs arising from increased free energy conservation in Saccharomyces cerevisiae*. Delft University of Technology. https://doi.org/10.4233/UUID:177E9F4C-F847-436D-9FD4-9ED97BA709D9

Sieuwerts, S. (2009). *Analysis of molecular interactions between yoghurt bacteria by an integrated genomics approach*. Wageningen University. https://search.proquest.com/openview/db5cc2850745b4df8f5f1d51cc0140be/1?pq-origsite=gscholar&cbl=2026366&diss=y

Sieuwerts, S., Molenaar, D., van Hijum, S. A. F. T., Beerthuyzen, M., Stevens, M. J. A., Janssen, P. W. M., Ingham, C. J., de Bok, F. A. M., de Vos, W. M., & van Hylckama Vlieg, J. E. T. (2010). Mixed-culture transcriptome analysis reveals the molecular basis of mixed-culture growth in *Streptococcus thermophilus* and *Lactobacillus bulgaricus*. *Applied and Environmental Microbiology*, *76*(23), 7775–7784. https://doi.org/10.1128/AEM.01122-10

Simensen, V., Schulz, C., Karlsen, E., Bråtelund, S., Burgos, I., Thorfinnsdottir, L. B., García-Calvo, L., Bruheim, P., & Almaas, E. (2022). Experimental determination of *Escherichia coli* biomass composition for constraint-based metabolic modeling. *PLoS ONE*, *17*(1), e0262450. https://doi.org/10.1371/journal.pone.0262450

Suzuki, I., Kato, S., Kitada, T., Yano, N., & Morichi, T. (1986). Growth of *Lactobacillus bulgaricus* in milk. 1. Cell elongation and the role of

formic acid in boiled milk. *Journal of Dairy Science*, *69*(2), 311–320. https://doi.org/10.3168/jds.S0022-0302(86)80407-6

Teusink, B., Wiersma, A., Molenaar, D., Francke, C., de Vos, W. M., Siezen, R. J., & Smid, E. J. (2006). Analysis of growth of *Lactobacillus plantarum* WCFS1 on a complex medium using a genome-scale metabolic model. *Journal of Biological Chemistry*, *281*(52), 40041–40048. https://doi.org/10.1074/jbc.M606263200

Ulusu, N. N. (2015). Evolution of enzyme kinetic mechanisms. *Journal of Molecular Evolution*, *80*(5–6), 251–257. https://doi.org/10.1007/s00239-015-9681-0

Uritskiy, G. V., DiRuggiero, J., & Taylor, J. (2018). MetaWRAP—A flexible pipeline for genome-resolved metagenomic data analysis. *Microbiome*, *6*(1), 158. https://doi.org/10.1186/s40168-018-0541-1

Vázquez, J. A., & Murado, M. A. (2008). Unstructured mathematical model for biomass, lactic acid and bacteriocin production by lactic acid bacteria in batch fermentation. *Journal of Chemical Technology*, *83*(1), 91–96. https://onlinelibrary.wiley.com/doi/abs/10.1002/jctb.1789

Vereecken, K. M., & Van Impe, J. F. (2002). Analysis and practical implementation of a model for combined growth and metabolite production of lactic acid bacteria. *International Journal of Food Microbiology*, *73*(2–3), 239–250. https://doi.org/10.1016/s0168-1605(01)00641-9

Wittig, U., Rey, M., Weidemann, A., Kania, R., & Müller, W. (2018). SABIO-RK: An updated resource for manually curated biochemical reaction kinetics. *Nucleic Acids Research*, *46*(D1), D656–D660. https://doi.org/10.1093/nar/gkx1065

Wood, D. E., Lu, J., & Langmead, B. (2019). Improved metagenomic analysis with Kraken 2. *Genome Biology*, *20*(1), 257. https://doi.org/10.1186/s13059-019-1891-0

Wu, L.-H., Lu, Z.-M., Zhang, X.-J., Wang, Z.-M., Yu, Y.-J., Shi, J.-S., & Xu, Z.-H. (2017). Metagenomics reveals flavour metabolic network of cereal vinegar microbiota. *Food Microbiology*, *62*, 23–31. https://doi.org/10.1016/j.fm.2016.09.010

Wu, Y.-W., Simmons, B. A., & Singer, S. W. (2016). MaxBin 2.0: An automated binning algorithm to recover genomes from multiple metagenomic datasets. *Bioinformatics*, *32*(4), 605–607. https://doi.org/10.1093/bioinformatics/btv638

Youssef, C. B., Goma, G., & Olmos-Dichara, A. (2005). Kinetic modelling of *Lactobacillus casei* ssp. *rhamnosus* growth and lactic acid production in batch cultures under various medium conditions. *Biotechnology Letters*, *27*(22), 1785–1789. https://doi.org/10.1007/s10529-005-3557-0

Yun, J. J., Barbano, D. M., Kiely, L. J., & Kindstedt, P. S. (1995). Mozzarella cheese: Impact of rod:coccus ratio on composition, proteolysis, and functional properties. *Journal of Dairy Science*, *78*(4), 751–760. https://doi.org/10.3168/jds.s0022-0302(95)76686-3

Zeng, H., & Yang, A. (2020). Bridging substrate intake kinetics and bacterial growth phenotypes with flux balance analysis incorporating proteome allocation. *Scientific Reports*, *10*(1), 4283. https://doi.org/10.1038/s41598-020-61174-0

SUPPORTING INFORMATION

Additional supporting information can be found online in the Supporting Information section at the end of this article.

How to cite this article: Qiu, S., Zeng, H., Yang, Z., Hung, W.-L., Wang, B., & Yang, A. (2023). Dynamic metagenome-scale metabolic modeling of a yogurt bacterial community. *Biotechnology and Bioengineering*, *120*, 2186–2198. https://doi.org/10.1002/bit.28492